

An ensemble based on a bi-objective evolutionary spectral algorithm for graph clustering

Camila P.S. Tautenhain and Mariá C.V. Nascimento

Instituto de Ciência e Tecnologia, Universidade Federal de São Paulo
São José dos Campos, Brasil
{santos.camila,mcv.nascimento}@unifesp.br

Preprint submitted to Expert Systems with Applications

Abstract

Graph clustering is a challenging pattern recognition problem whose goal is to identify vertex partitions with high intra-group connectivity. Because of the rough definition of this problem, there are numerous effective ways to formally determine such partitions. In particular, multi-objective optimization can deal with the trade-offs between different clustering quality measures in order to better assess the partitions. This paper investigates a problem that maximizes the number of intra-cluster edges of a graph and minimizes the expected number of inter-cluster edges in a random graph with the same degree sequence as the original one. The difference between the two investigated objectives is the definition of the well-known measure of graph clustering quality: the modularity. We introduce a spectral decomposition hybridized with an evolutionary heuristic, called *MOSpecG*, to approach this bi-objective problem and an ensemble strategy to consolidate the solutions found by *MOSpecG* into a final robust partition. The results of computational experiments with real and artificial LFR networks demonstrated a significant improvement in the results and performance of the introduced method in regard to another bi-objective algorithm found in the literature.

Keywords: Graph clustering, Community detection, Evolutionary heuristic, Multi-objective optimization, Modularity maximization

1 Introduction

The majority of graphs that describe real networks, such as social and metabolic networks [29, 17], are characterized by vertex partitions with high intra-cluster connectivity [10]. The

graph clustering problem aims at identifying such partitions. The definition of the problem, nevertheless, is biased towards the assessment criterion of graph clusterings.

Modularity maximization is one of the most popular criteria to define graph clusterings. The modularity of a partition is the difference between the number of edges in the same groups (first term) and the expected number of edges within the groups in a random graph with the same vertex degree sequence as the original graph (second term) [22]. However, many studies in the literature point out that by simply defining the measure as the difference between these two terms, without scaling them, may be a poor way to evaluate graph clusterings [9, 24].

As an attempt to mitigate this scaling problem, Reichardt and Bornholdt [24] suggested multiplying the second term of the modularity measure by a parameter called resolution parameter. A few studies approaching this modified modularity have shown interesting results [26, 3]. Carvalho et al. [3], for example, introduced a supervised method that automatically adjusts the resolution parameter based on the graph topology. The method was later employed in the consensus algorithm proposed by Santos et al. [26]. In spite of the potential of the strategies, they require labeled data for defining a training set of the supervised algorithm. Berry et al. [1], De Meo et al. [6] and Khadivi et al. [12] introduced pre-processing strategies to change the edge weights of a graph in order to diminish the negative effects of the resolution limit without the prior knowledge of the resolution parameter.

Another approach that explores the duality between the first and second terms of the modularity measure was introduced by Shi et al. [27]. The authors introduced an evolutionary algorithm called MOCD for solving the bi-objective problem that maximizes the first term of modularity and minimizes the second term of modularity. MOCD achieved good quality partitions when compared to the other evolutionary bi-objective clustering algorithm, known as Moga-Net [23].

This paper investigates a weighted aggregation method for solving the bi-objective problem that optimizes the first and second terms of modularity. The resulting problem is here called weighted aggregate modularity and is equivalent to solving the problems that maximize the modularity with different resolution parameter values, as demonstrated in this paper. To solve the weighted aggregate modularity, we propose a multi-objective evolutionary algorithm whose fitness function is the spectral relaxation of the weighted aggregate modularity matrix. In addition, we explore the close relationship between multi-objective clusterings and ensemble clusterings by introducing an ensemble of the approximation of the Pareto solutions that adjusts the edge weights of the graph.

Thereby, the proposed algorithm deals with the resolution limit by combining both the edge weighting and resolution parameter strategies, without the need of predefining the resolution parameter. Furthermore, we estimate an upper bound to the number of clusters in

advance, which might contribute to further reductions of the negative effects of the resolution limit according to the computational experiments performed by Darst et al. [5].

Computational experiments were carried out using real and LFR networks [16]. The proposed algorithm outperformed the multi-objective algorithm Moga-Net in all the networks and was from 6 to 64 times faster in the LFR networks. Despite the slightly better results achieved by the reference mono-objective algorithms Order Statistics Local Optimization Method (OSLOM) [17] and Infomap [25] in most of the LFR networks, the proposed algorithm outperformed them in the LFR networks with large mixture coefficients.

The rest of this paper is organized as follows: Section 2 presents a brief literature review of multi-objective and ensemble graph clustering algorithms; Section 3 thoroughly describes the studied spectral decomposition of the weighted aggregate modularity; Section 4 introduces the multi-objective evolutionary algorithm proposed in this paper; Section 5 discusses the computational experiments carried out with the algorithm in question along with the analysis of the results; and, to sum up, Section 6 briefly summarizes the contributions of the paper and outlines further works.

2 Related Works

Graph clustering algorithms usually optimize quality measures to find vertex partitions. Some examples of measures employed in such optimization are the modularity measure [22], the clustering coefficient measure [28] and map equation [25]. Conceptually different measures to define groups of highly related vertices exist due to the difficulty in theoretically defining a graph clustering. When optimizing a quality measure, algorithms may work fairly well in detecting graph clustering in networks with a given structure, but poorly in other networks. To mitigate the bias of algorithms that optimize a single quality measure, some algorithms in the literature are founded on ensemble clustering and multi-objective optimization.

Multi-objective optimization involves solving problems with two or more conflicting objective functions. The existence of trade-offs amongst objective functions is the reason why a single solution cannot optimize all the functions simultaneously; instead, a number of efficient solutions, known as Pareto solutions, describes the best solutions for adequate decision-making. In a multi-objective problem, a solution is called efficient when it is not possible to improve the value of any objective function without worsening the value of another function.

There are numerous multi-objective algorithms focusing on graph clustering [23, 27, 11, 30], even though most methods concern data clustering. Because of the computational challenges involved in graph partitioning problems, especially in large-scale networks, many of

these algorithms are heuristics. In particular, the overwhelming majority of multi-objective graph clustering solution methods are evolutionary algorithms, due to the set of evolved solutions provided by their population-based structure.

Pizzuti [23] introduced a multi-objective genetic algorithm, which the authors named Moga-Net, whose objective functions involve maximizing and minimizing, respectively, the in-degree and out-degree of clusters. In computational experiments with large real networks, the modularity values of the best modularity valued partitions from the Pareto sets found by Moga-Net were worse than those found by a mono-objective spectral clustering algorithm in the literature.

Similar to Shi et al. [27], who introduced MOCD, mentioned in the earlier section of this paper, Gong et al. [11] and Žalik and Žalik [30] also optimized the two terms of the modularity measure using multi-objective evolutionary algorithms. In particular, the partitions with the highest modularity values found by the algorithm introduced by Gong et al. [11], called MOEA/D-Net, outperformed classical graph clustering algorithms, such as Infomap, in the artificial instances.

Ensemble and consensus clustering are both solution methods that combine algorithms, partitions or models to perform the clustering task. These methods have been intensively studied in the last decades [20, 15, 26]. They tend to be more robust than those that optimize a single criterion.

The ensemble algorithms for graph clustering related to the study performed in this paper belong to the class of ensemble methods that combines partitions from a set of diverse partitions in order to determine a consensus partition. The strategy to define such consensus partitions relies on observing whether a pair of vertices is in the same group in most of the partitions in the set. Studies [15] and [26] obtained good results using these methods.

3 Weighted Aggregate Modularity

This section discusses the spectral decomposition of the weighted aggregate modularity. Throughout this paper, let $G = (V, E)$ be an undirected graph, where V is its set of n vertices and E is its set of m edges. The edges of G are unordered pairs of distinct adjacent vertices (i, j) , where $i, j \in V$. Let $A = [a_{ij}] \in \mathbb{N}^{n \times n}$ be the adjacency matrix of G , i.e., a_{ij} is the weight of edge (i, j) if $(i, j) \in E$, and 0 otherwise. The degree of a vertex i , d_i , is given by $\sum_{j \in V} a_{ij}$. A vertex partition with k clusters (groups or communities) is here defined as $\mathcal{C} = \{C_1, C_2, \dots, C_k\}$, where $\bigcup_{t=1}^k C_t = V$ and $C_t \cap C_{t'} = \emptyset, \forall t \neq t' \in \{1, 2, \dots, k\}$. The label of a cluster C_t is t and, for ease of notation, we refer to cluster C_t as the cluster with label t and to the label of the cluster of a vertex i in a partition \mathcal{C} as $\mathcal{C}(i)$.

Modularity is a measure that assesses the difference between the number of edges within

clusters and its expected number in a random graph with the same degree sequence as the graph under consideration. Equation (1) presents a way to calculate the modularity measure originally introduced by Newman and Girvan [22].

$$Q(\mathcal{C}) = \frac{1}{2m} \sum_{i,j \in V} \left(a_{ij} - \frac{d_i d_j}{2m} \right) \delta_{\mathcal{C}(i), \mathcal{C}(j)} \quad (1)$$

In Equation (1), $\delta_{\mathcal{C}(i), \mathcal{C}(j)}$ is an indicator function that assumes value 1 if $\mathcal{C}(i) = \mathcal{C}(j)$, and 0 otherwise. The resolution parameter, as suggested by Reichardt and Bornholdt [24], is a scalar γ that multiplies the term $\frac{d_i d_j}{2m}$ in Equation (1).

Equation (1) shows that in order to maximize the modularity, the first term, i.e. a_{ij} , must be maximized and the second term, i.e. $\frac{d_i d_j}{2m}$, has to be minimized. On the one hand, the higher the number of edges within clusters, the higher the first term. On the other, the lower the number of edges within clusters, the lower the expected number of edges within clusters and consequently, the lower the second term. These two terms, therefore, are conflicting and result in a trade-off in the modularity measure [2].

As discussed earlier in this paper, Shi et al. [27] have approached the bi-objective problem that optimizes the two terms of modularity. Equations (2) and (3) present the pair of objective functions of the bi-objective problem.

$$\max_{\mathcal{C}} Q^{IN}(\mathcal{C}) = \frac{1}{2m} \sum_{i,j \in V} a_{ij} \delta_{\mathcal{C}(i), \mathcal{C}(j)} \quad (2)$$

$$\min_{\mathcal{C}} Q^{NULL}(\mathcal{C}) = \frac{1}{2m} \sum_{i,j \in V} \frac{d_i d_j}{2m} \delta_{\mathcal{C}(i), \mathcal{C}(j)} \quad (3)$$

Consider the weighted aggregation of the objective functions $Q^{IN}(\mathcal{C})$ and $Q^{NULL}(\mathcal{C})$ as presented in Equation (4). The objective function (3) can be transformed into a maximization function without loss of generality by multiplying the function by -1.

$$QW(\mathcal{C}) = \frac{1}{2m} \sum_{i,j \in V} \left[\gamma_1 a_{ij} - \gamma_2 \frac{d_i d_j}{2m} \right] \delta_{\mathcal{C}(i), \mathcal{C}(j)}, \quad (4)$$

where $\gamma_1, \gamma_2 \in \mathbb{R}, \gamma_1 + \gamma_2 = 1$.

The set of solutions for the weighted aggregation problem for different values of γ_1 and γ_2 are efficient [8], and thereby provide an approximation to the Pareto frontier of the bi-objective problem. Moreover, as γ_1 and γ_2 are both scalars, when $\gamma_1 > 0$ the optimization problem $\max_{\mathcal{C}} QW$ is equivalent to $\frac{1}{\gamma_1} \max_{\mathcal{C}} QW$, which is exactly the adjusted modularity maximization problem. Therefore, the solutions of the modularity maximization problem with different values of resolution parameter are also efficient Pareto solutions for the bi-objective problem (2)-(3). In particular, the maximization of Equation (4) for $\gamma_1 = \gamma_2 = 0.5$

is equivalent to the classical modularity maximization problem.

3.1 Spectral decomposition

This section presents the spectral decomposition of the weighted aggregation of modularity provided in Equation (4). It is strongly based on the spectral decomposition proposed by Newman [21]. Let us first define in Equation (5) the weighted aggregate matrix $BW = [bw_{ij}] \in \mathbb{R}^{n \times n}$.

$$bw_{ij} = \gamma_1 a_{ij} - \gamma_2 \frac{d_i d_j}{2m} \quad (5)$$

Note that the modularity matrix is $B = \frac{1}{\gamma_1} BW$, where $\gamma = \frac{\gamma_2}{\gamma_1} = 1$. Consider the sequence of eigenvalues of matrix BW , $\lambda_1, \lambda_2, \dots, \lambda_n$, sorted in the decreasing order of absolute value, that is, $|\lambda_1| \geq |\lambda_2| \geq \dots \geq |\lambda_n|$. Let $U \in \mathbb{R}^{n \times n}$ be a matrix such that its j -th column, referred to as column u_j , is an eigenvector of BW associated with eigenvalue λ_j . BW is symmetric and thus admits an eigen-decomposition: $BW = U\Lambda U^T$, where $\Lambda = [\Lambda_{ij}] \in \mathbb{R}^{n \times n}$ is a diagonal matrix such that $\Lambda_{ii} = \lambda_i$.

Let $S = [s_{it}] \in \mathbb{N}^{n \times k}$ be a binary matrix associated with a solution of the graph clustering problem. Element s_{it} receives 1 if vertex i belongs to cluster C_t , and 0 otherwise. Therefore, $\delta(\mathcal{C}(i), \mathcal{C}(j)) = \sum_{t=1}^k s_{it} s_{jt}$. Equation (4) can hence be rewritten as indicated in Equation (6).

$$QW(\mathcal{C}) = \frac{1}{2m} \sum_{i,j \in V} \sum_{t=1}^k bw_{ij} s_{it} s_{jt} = \frac{1}{2m} \text{Tr}(S^T BWS) \quad (6)$$

Any given vertex belongs to exactly and only one cluster, which implies that $\sum_{t=1}^k s_{it} = 1, i = 1, \dots, n$, and $\text{Tr}(S^T S) = n$. Knowing that U is an orthogonal matrix, we can rewrite Equation (6) as Equation (7).

$$QW(\mathcal{C}) = \frac{1}{2m} \text{Tr}[S^T U \Lambda U^T S] = \frac{1}{2m} \sum_{j=1}^n \sum_{t=1}^k \lambda_j \left(\sum_{i=1}^n u_{ij} s_{it} \right)^2 \quad (7)$$

Since Equation (7) shows that only positive eigenvalues increase the value of QW , Newman [21] suggested approximating Equation (7) using only the first largest positive eigenvalues. Nonetheless, Newman [21] also demonstrated that negative eigenvalues are important to indicate vertices that decrease the $QW(\mathcal{C})$ in case they are clustered together. This paper takes into account the negative eigenvalues by selecting the first p eigenvalues sorted in decreasing order of absolute value.

Consider \mathcal{E} the set of the first p eigenvalues of BW ; let $\mathcal{E}p = \{j | \lambda_j \in \mathcal{E} \text{ such that } \lambda_j \geq 0\}$

and $\mathcal{E}_n = \{j | \lambda_j \in \mathcal{E} \text{ such that } \lambda_j < 0\}$ be the positive and negative eigenvalue indices, respectively. Moreover, let $rp^i \in \mathbb{R}^p$ and $rn^i \in \mathbb{R}^p$ be the vectors regarding vertex i whose components are defined by Equations (8) and (9), respectively. Also, in this paper, rp^i is called positive vector of vertex i , whereas rn^i is referred to as negative vector of vertex i .

$$rp_j^i = \begin{cases} \sqrt{\lambda_j} u_{ij} & , \text{ if } j \in \mathcal{E}_p \\ 0 & , \text{ if } j \in \mathcal{E}_n \end{cases} \quad (8)$$

$$rn_j^i = \begin{cases} \sqrt{-\lambda_j} u_{ij} & , \text{ if } j \in \mathcal{E}_n \\ 0 & , \text{ if } j \in \mathcal{E}_p \end{cases} \quad (9)$$

Equation (10) approximates Equation (7) using the p largest eigenvalues in absolute value.

$$\begin{aligned} QW(\mathcal{C}) &\simeq \frac{1}{2m} \sum_{\lambda_j \in \mathcal{E}} \sum_{t=1}^k \left[\sum_{i=1}^n \sqrt{|\lambda_j|} u_{ij} s_{it} \right]^2 \\ &= \frac{1}{2m} \sum_{t=1}^k \sum_{j=1}^p \left[\left(\sum_{i \in C_t} rp_j^i \right)^2 - \left(\sum_{i \in C_t} rn_j^i \right)^2 \right] \\ &= \frac{1}{2m} \sum_{t=1}^k (\|Rp^t\|^2 - \|Rn^t\|^2) \end{aligned} \quad (10)$$

where $\forall j \in \{1, \dots, p\}$, $Rp_j^t = \sum_{i \in C_t} rp_j^i$ and $Rn_j^t = \sum_{i \in C_t} rn_j^i$.

Furthermore, $Rp^t = [Rp_j^t]_{j=1 \dots p}$ and $Rn^t = [Rn_j^t]_{j=1 \dots p}$ are referred to as vectors of cluster C_t . In this paper, Rp^t is called positive vector of cluster C_t , whereas Rn^t is referred to as negative vector of cluster C_t .

Similarly to the results of the approximation with positive eigenvalues carried out by Newman [21], we have reduced the weighted aggregate modularity maximization problem into a vector partitioning problem. The goal of the vector partitioning problem is to find a vertex partition by maximizing the terms Rp^t and minimizing the terms Rn^t , for $t = 1, 2, \dots, k$.

It is well-known that the number of groups has a direct impact on the number of eigenvectors required to determine graph clusterings. Thereby, most spectral heuristics must first define the number of groups, which is generally not known in advance.

3.2 Defining the number of clusters

In this paper, we adapted the strategy to identify the number of clusters presented by Krzakala et al. [14], who constructed a matrix called non-backtracking-matrix from the adjacency matrix of a given graph, and estimated the number of clusters through the eigenvalues of this matrix.

The adaptation proposed here consists in estimating the number of clusters based on the weighted aggregate modularity matrix BW . Let χ be the largest (leading) eigenvalue of BW . The proposed algorithm sets k' as the number of eigenvalues of BW higher than $\sqrt{\chi}$. In this paper, we estimate the number of clusters, k , to be $\lfloor 1.25k' \rfloor$. This estimation is an upper bound to the number of clusters because the proposed algorithm might leave one or more clusters empty.

Figure 1 displays an example of the proposed strategy by depicting the eigenvalues of the Karate network, whose largest eigenvalue is 4.977. The red squares in this figure indicate the points $(-\sqrt{\chi}, 0)$ and $(\sqrt{\chi}, 0)$ and a circumference of radius $\sqrt{\chi}$ centered at the origin of the Cartesian plane. Most of the black dots, which correspond to the eigenvalues of matrix BW , are enclosed by the circumference. The proposed algorithm estimates k' to be the number of eigenvalues higher than $\sqrt{\chi}$, i.e., the number of positive points outside the circumference, which is 3. Therefore, the upper bound estimation to the number of clusters is $k = 3$.

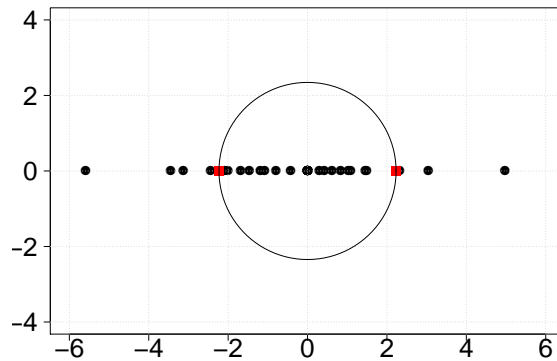


Figure 1: Distribution of the eigenvalues of the Karate network.

3.3 Geometric interpretation

Figure 2 illustrates, for a given bipartition of the benchmark Karate network [29], the geometric interpretation of all the vectors of vertices and clusters. This network has 34 vertices. The positive and negative vectors are shown in Figures 2(a) and 2(b), respectively. In these figures, the vectors of clusters are identified by their labels and the solid and dashed lines distinguish the vertex vectors regarding clusters 1 and 2, respectively.

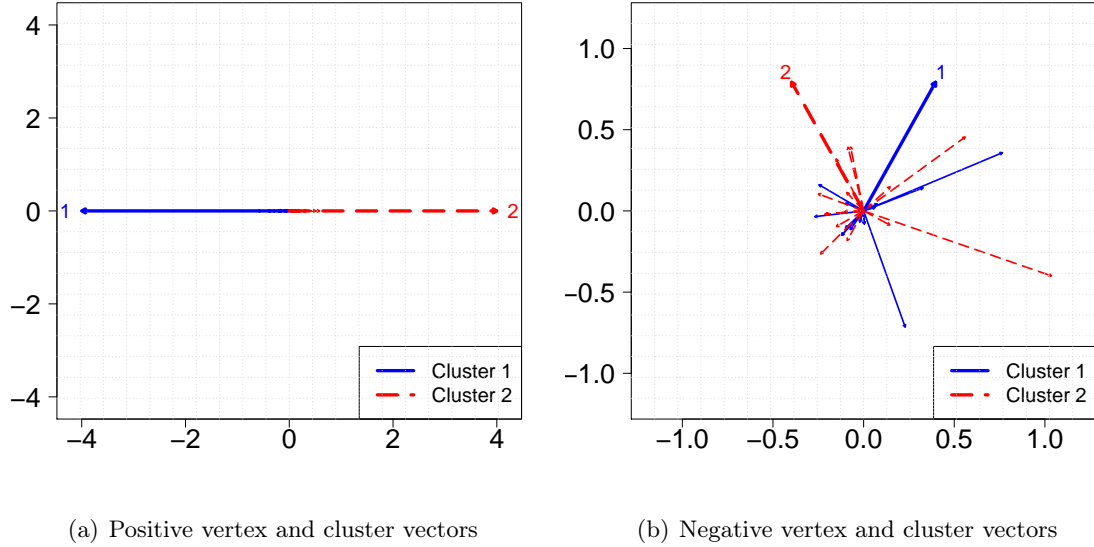


Figure 2: Vectors of the vertices and clusters of the bipartition found by the algorithm proposed in this paper to maximize the weighted aggregate modularity with $\gamma_1 = \gamma_2 = 0.5$ applied to the Karate network.

The cluster vectors are the sum of the vertex vectors that compose the clusters. The higher $Rp^{tT}rp^i$ and the lower $Rn^{tT}rn^i, \forall i \in V$ and $t = \mathcal{C}(i)$, the higher the modularity. On the one hand, the obvious choice to maximize the magnitude of the positive cluster vectors in Figure 2(a) is to select the vertices whose positive vertex vectors point to the same direction. On the other hand, to minimize the magnitude of the negative cluster vectors in Figure 2(b), the vertices whose negative vertex vectors point to opposite directions should be selected. By comparing Figures 2(a) and 2(b), it is possible to observe that the magnitude of the positive vectors of the clusters is approximately 4.51 times higher than the magnitude of the negative vectors of the clusters.

3.4 Moving vertices between clusters

Given a partition \mathcal{C} at hand, some procedures attempt to enhance its quality, which can be evaluated using a fitness function. One way of performing this task is by moving vertices from one cluster to another so that the modified partition has a better quality than the previous one. Many studies that employ this type of strategy can be found in the literature, e.g. [21] and [31].

Moving a vertex i from a cluster C_b to a cluster C_t modifies the fitness function value, i.e., the weighted aggregate modularity. Let the vectors of clusters C_b and C_t , disregarding

the contribution of vertex i , be defined by $Rp^b = \sum_{v \in C_b, v \neq i} rp^v$, $Rn^b = \sum_{v \in C_b, v \neq i} rn^v$, $Rp^t = \sum_{v \in C_t} rp^v$ and $Rn^t = \sum_{v \in C_t} rn^v$.

On the one hand, before moving i to cluster C_t , the vectors of clusters C_b are given by $Rp^b = Rp^b + rp^i$ and $Rn^b = Rn^b + rn^i$, respectively. On the other hand, before any movement, the vectors of cluster C_t are $Rp^t = Rp^t$ and $Rn^t = Rn^t$. After moving i from cluster C_b to C_t , the vectors of the clusters are $Rp^{''b} = Rp^b$, $Rp^{''t} = Rp^t + rp^i$, $Rn^{''b} = Rn^b$ and $Rn^{''t} = Rn^t + rn^i$. Equation (11) presents the change in the weighted aggregate modularity of partition \mathcal{C} after moving a vertex i from a cluster C_b to a cluster C_t .

$$\begin{aligned} \Delta QW(i, C_b, C_t) &= \frac{1}{2m} [\|Rp^{''b}\|^2 - \|Rn^{''b}\|^2 + \|Rp^{''t}\|^2 - \|Rn^{''t}\|^2 \\ &\quad - (\|Rp^{''b}\|^2 - \|Rn^{''b}\|^2 + \|Rp^t\|^2 - \|Rn^t\|^2)] \\ &= \frac{1}{m} [Rp^{tT} rp^i - Rn^{tT} rn^i - Rp^{bT} rp^i + Rn^{bT} rn^i] \end{aligned} \quad (11)$$

From Equation (11), it is possible to see that $\Delta QW(i, b, t) \geq 0$ if $(Rp^{tT} rp^i - Rn^{tT} rn^i) \geq (Rp^{bT} rp^i - Rn^{bT} rn^i)$.

Recently, Zhang and Newman [31] presented a spectral greedy heuristic to solve the vector partitioning problem considering only positive eigenvalues. In this heuristic, starting from an initial group of vectors, at each iteration, the algorithm moves a vertex i to the cluster C_{t^*} that results in the largest positive gain in modularity. Concerning both positive and negative eigenvalues, a simple greedy heuristic consists of moving vertex i to the cluster C_{t^*} that results in the largest value for $Rp^{t^*T} rp^i - Rn^{t^*T} rn^i$. Equation (12) defines the choice of t^* .

$$t^* = \arg \max_{t \in \{1, \dots, k\}} \begin{cases} Rp^{tT} rp^i - Rn^{tT} rn^i & , \text{ if } \mathcal{C}(i) \neq t \\ 0 & , \text{ if } \mathcal{C}(i) = t \end{cases} \quad (12)$$

If $t^* = \mathcal{C}(i)$, vertex i will remain in its original cluster.

4 Proposed evolutionary algorithm

This section thoroughly describes the evolutionary multi-objective algorithm proposed in this paper and called *MOSpecG*. Before going into detail on the algorithm, let us briefly introduce some basic concepts and notations on evolutionary and genetic algorithms.

Evolutionary algorithms are heuristics based on the natural evolution theory [7]. Genetic algorithms (GA), in particular, have been successfully applied to a plethora of optimization

problems, among which multi-objective community detection problems [23, 11, 30].

GAs are based on the iterative improvement of a set of solutions, called population. A solution to a target problem is also referred to as an individual and is evaluated through a problem-specific fitness function. Each iteration of a GA is a generation and employs procedures based on genetic operators such as crossover, mutation and selection to evolve the current population to the next generation. The crossover operator generates new offspring individuals by combining two individuals: the parents. Moreover, the mutation operator randomly performs perturbations on the individuals; and the selection operator is responsible for selecting the fittest individuals to form the population of the next generation.

Memetic Algorithms (MA) are Evolutionary Algorithms that are strongly based on GAs. The main difference between them is that MAs employ problem-specific operators, such as local search procedures, to improve the fitness of a population along the generations.

The proposed algorithm, *MOSpecG*, is an MA whose fitness function is the weighted aggregate modularity presented in Equation (4). In *MOSpecG*, the population of the g -ith generation is defined by $\mathcal{P}^g = \{P_1^g, P_2^g, \dots, P_{N\mathcal{P}}^g\}$, where $g \in \{1, 2, \dots, N\mathcal{G}\}$. The individuals from the population of the g -ith generation are the partitions P_h^g , $h \in \{1, 2, \dots, N\mathcal{P}\}$. Starting from an initial population, each generation of *MOSpecG* (i) constructs a new offspring population with individuals from the current population by applying the crossover operator; (ii) perturbs the offspring population with the mutation operator; and (iii) attempts to enhance the fitness of the offspring population with the local search procedure. At the end of each generation, the fittest individuals in the offspring population replace the individuals with the lowest fitness values in the current population.

4.1 Multi-objective spectral algorithm

Algorithm 1 introduces the *MOSpecG*, which has an undirected unweighted graph G as input; the size of the Pareto frontier, $N\mathcal{F}$; the number of generations, $N\mathcal{G}$; the number of solutions in the population, $N\mathcal{P}$; the percentage of solutions from the offspring, $N\mathcal{O}$; the number of eigenvalues and eigenvectors to be computed, p ; and the number of iterations of the local search procedure, IT .

In line 1 of Algorithm 1, set \mathcal{F} is initialized as empty. Line 2 assigns the grid spacing to variable *inc* in order to define values for γ_1 . The grid spacing is dependent on the number of solutions of the resulting Pareto frontier to guarantee a good spacing between the solutions found by the algorithm. In the sequence, weight γ_2 is calculated taking γ_1 as reference, in line 4. From lines 5 to 11, the proposed heuristic creates a new solution to the approximation of the Pareto frontier by optimizing QW with the current values of γ_1 and γ_2 .

In particular, in line 5, the algorithm constructs matrix BW with weights γ_1 and γ_2 according to Equation (5). To implement the computation of the largest p eigenvalues and

the respective eigenvectors that compose Λ and U required in line 6, the algorithm used the *implicitly restarted Arnoldi method* from ARPACK++ library [18]. In line 7, the leading eigenvalue is assigned to χ . In lines 8 and 9, the proposed heuristic estimates the number of clusters, k , according to Section 3.2.

In line 10, the algorithm defines vertex vectors rp^i and rn^i , $\forall i \in V$, as in Equations (8) and (9), respectively. In line 11, *MOSpecG* calls the *Memetic Algorithm* function presented in Algorithm 2 to optimize QW with weights γ_1 and γ_2 and updates the Pareto frontier approximation \mathcal{F} in line 12. At the end, Algorithm 1 returns \mathcal{F} .

Algorithm 1: *MOSpecG*

Input : $G, \mathcal{NF}, \mathcal{NG}, \mathcal{NP}, \mathcal{NO}, p$ and IT
Output: \mathcal{F}

- 1 $\mathcal{F} = \emptyset$
- 2 $inc = \frac{1}{\mathcal{NF}-1}$
- 3 **for** $\gamma_1 = 0$ to 1, $\gamma_1 = \gamma_1 + inc$ **do**
- 4 $\gamma_2 = 1 - \gamma_1$
- 5 Construct the weighted aggregate modularity matrix BW with weights γ_1 and γ_2
- 6 $\Lambda, U :=$ Eigen-decomposition of BW regarding the p largest eigenvalues in absolute value
- 7 $\chi := \max_{\Lambda_{ii}, \forall i} (\Lambda_{ii})$
- 8 $k' :=$ number of eigenvalues of BW with value larger than or equal to $\sqrt{\chi}$
- 9 $k := \lfloor 1.25k' \rfloor$
- 10 Define vertex vectors rp^i and rn^i , $\forall i \in V$
- 11 $\mathcal{C} :=$ *Memetic Algorithm*($\mathcal{NG}, \mathcal{NP}, \mathcal{NO}, IT, k, rp^i, rn^i, \forall i \in V$)
- 12 $\mathcal{F} := \mathcal{F} \cup \mathcal{C}$
- 13 **end**

Algorithm 2 presents the proposed *Memetic Algorithm*, whose inputs are: \mathcal{NG} ; \mathcal{NP} ; \mathcal{NO} ; IT ; the number of clusters, k ; and the vertex vectors rp^i and rn^i , $\forall i \in V$. In line 1 of Algorithm 2, the initial population, i.e., individuals from the first generation, is constructed using the strategy suggested by Zhang and Newman [31]: it selects k vertices and assigns each of them to a different cluster (k singletons). Then, the vectors of clusters Rp^t and Rn^t , $t = 1, \dots, k$, are updated and the remaining vertices are assigned to clusters C_{t^*} , where t^* is chosen according to Equation (12).

Figure 3 shows an example of an initial partition of the Karate network. To calculate QW , we considered $\gamma_1 = \gamma_2 = 0.5$. In this figure, each square identifies the cluster label of a vertex of the network.

For a given generation g , the *Memetic Algorithm* - line 3 - constructs an offspring, \mathcal{O} , by applying the genetic operator crossover (Algorithm 3) to the current population \mathcal{P}^g . In lines 4 and 5, the genetic operator mutation (Algorithm 4) and a local search procedure

Algorithm 2: Memetic Algorithm

Input : NG, NP, NO, IT, k, rp^i and $rn^i, \forall i \in V$
Output: Fittest individual C^*

- 1 $P_s^1, s = 1, \dots, NP :=$ construct solution using vertex vectors as directions
- 2 **for** $g = 1$ to NG **do**
- 3 $\mathcal{O} := \text{Crossover}(\mathcal{P}^g, k, rp^i, rn^i, \forall i \in V)$
- 4 $\mathcal{O} := \text{Mutation}(\mathcal{O}, k, rp^i, rn^i, \forall i \in V)$
- 5 $\mathcal{O} := \text{LocalSearch}(\mathcal{O}, k, rp^i, rn^i, \forall i \in V)$
- 6 $\mathcal{P}^{g+1} :=$ Update population \mathcal{P}^g using \mathcal{O}
- 7 **end**
- 8 $\mathcal{P}^* :=$ the fittest individual from \mathcal{P}^{NG}

P_s^1

1	2	1	1	1	1	1	1	1	1	1	1	1	1	1	2	2	1	1	2	1	2	1	2	2	2	2	2	2	2	2	2	2	2	2	2	2	2
---	---	---	---	---	---	---	---	---	---	---	---	---	---	---	---	---	---	---	---	---	---	---	---	---	---	---	---	---	---	---	---	---	---	---	---	---	---

 $QW(P_s^1) = 0.1443$

Figure 3: Example of a solution for the Karate network when $\gamma_1 = \gamma_2 = 0.5$.

(Algorithm 5) update the offspring population. The $NO\%$ fittest individuals from \mathcal{O} replace the $NO\%$ least fit individuals from the current population, \mathcal{P}^g , in order to construct the population of the next generation, \mathcal{P}^{g+1} , in line 6. In line 8, the algorithm returns the fittest individual from \mathcal{P}^{NG} , i.e., individual P^* such that $P^* = \arg \max_{P \in \mathcal{P}^{NG}} QW(P)$.

4.2 Crossover procedure

Algorithm 3 presents the one-way crossover procedure of the *Memetic Algorithm*, which has \mathcal{P}^g, k, rp^i and rn^i as input, $\forall i \in V$. At each iteration f , the crossover constructs a new solution for the offspring population, \mathcal{O} , by combining two solutions from the current population \mathcal{P}^g . In line 2, the fitness proportionate roulette method selects two individuals P_b^g and $P_d^g, b, d \in \{1, 2, \dots, NP\}, b \neq d$, to then perform the crossover. In line 3, the algorithm creates an offspring individual W as a copy of P_d^g . In line 4, the method randomly selects a vertex vs and, in line 5, ls stores the label of the cluster of vs in individual P_b^g .

In line 6, the crossover procedure selects the cluster with label ld^* from individual P_d^g as the cluster whose sum of the inner products $Rp_{ls}^b{}^T Rp_{ld}^d$ and $Rn_{ls}^b{}^T Rn_{ld}^d$ is the maximum amongst all $ld \in \{1, \dots, k\}$, according to Equation (13).

$$ld^* = \arg \max_{ld \in \{1, \dots, k\}} (Rp_{ls}^b{}^T Rp_{ld}^d + Rn_{ls}^b{}^T Rn_{ld}^d) \quad (13)$$

Figure 4 shows an example of the selection performed in line 6 of Algorithm 3 by illustrating the cluster vector with label $ls = 2$ in individual P_b^g , as a solid red line, and the

Algorithm 3: Crossover

Input : \mathcal{P}^g , k , rp^i and rn^i , $\forall i \in V$
Output: $\mathcal{O} = \{O_1, O_2, \dots, O_{N\mathcal{P}}\}$

- 1 **for** $f = 1$ to $N\mathcal{P}$ **do**
- 2 Pick randomly P_b^g and P_d^g , $b, d \in \{1, 2, \dots, N\mathcal{P}\}$, $b \neq d$, from \mathcal{P}^g with probability distribution $pr(P_h^g) = \frac{QW(P_h^g)}{\sum_{P_j^g \in \mathcal{P}} QW(P_j^g)}$, $h \in \{1, 2, \dots, N\mathcal{P}\}$.
- 3 $W := P_d^g$
- 4 Randomly select a vertex vs from V
- 5 $ls := P_b^g(vs)$
- 6 $ld^* :=$ choose according to Equation (13)
- 7 Move vd to cluster C_{ld^*} in individual W , $\forall vd \in V$ such that $P_b^g(vd) = ls$ and $W(vd) \neq ld^*$
- 8 Update QW and cluster vectors
- 9 $\mathcal{O}_f := W$
- 10 **end**

cluster vectors with labels $ld \in \{1, 2\}$ in individual P_d^g – candidates to ld^* – as dashed lines. The positive and negative vectors are identified by the label of the clusters and are shown in Figures 4(a) and 4(b), respectively. The conjecture that justifies the selection choice is that the clusters whose vectors point to the same direction have more vertices in common. In this example, the cluster with label $ld^* = 1$ from individual P_d^g is selected because the sum of the inner products between its positive and negative cluster vectors and the respective cluster vectors of $ls = 2$ in individual P_b^g is higher than the inner products of these vectors with the vectors of cluster $ld = 2$.

In line 7, the method moves the vertices vd in the cluster labeled ls in individual P_b^g to cluster labeled ld^* in individual W . For all $vd \in V$ already belong to the cluster labeled ld^* , nothing is done. After each movement, line 8 of Algorithm 3 updates the weighted aggregate modularity according to Equation (11) and the vectors of the clusters involved in the vertex moves in individual W , according to Section 3.4. After setting W as the offspring individual \mathcal{O}_f in line 9, the crossover returns the offspring population $\mathcal{O} = \{\mathcal{O}_1, \mathcal{O}_2, \dots, \mathcal{O}_{N\mathcal{P}}\}$.

Figure 5 gives an example of the crossover procedure when $\gamma_1 = \gamma_2 = 0.5$. In the example, the offspring individual W had a higher weighted aggregate modularity value than the parent individual P_d^1 . Let $ls = 2$; the selection of $ld^* = 1$ was illustrated in Figure 4. The vertices whose cluster label is $ls = 2$ on individual P_b^1 are in bold on the partitions. At the offspring individual, which is initially a copy of P_d^1 , these vertices are moved to the group labeled $ld^* = 1$, if they are not yet in this group.

4.3 Mutation procedure

Algorithm 4 presents the mutation procedure whose inputs are the offspring population, \mathcal{O} ; k ; rp^i and rn^i , $\forall i \in V$. In line 1, a random integer number in the interval $[1, \lfloor \frac{n}{2} \rfloor]$ is assigned to $count$, which indicates the number of mutations. In line 2, an individual O_d is randomly selected from \mathcal{O} and, in line 3, the algorithm picks $count$ vertices from V at random to define the set of vertices to be mutated, V' . Each vertex $vd \in V'$ is assigned to a cluster C_r chosen randomly from individual O_d , in lines 5 and 6. Note that if a cluster C_t is empty, vd will be assigned to a new cluster. After each movement of a vertex vd , both QW and the vectors of cluster C_r are updated in line 8. The mutation procedure halts when all vertices of V' have been mutated and, then, returns the updated offspring \mathcal{O} .

Algorithm 4: Mutation

Input : \mathcal{O} , k , rp^i and rn^i , $\forall i \in V$

Output: Updated \mathcal{O}

- 1 Randomly choose an integer number $count$ from interval $[1, \lfloor \frac{n}{2} \rfloor]$ with uniform probability distribution
 - 2 Randomly select an individual O_d from \mathcal{O}
 - 3 Randomly pick $count$ distinct elements from V and assign them to V'
 - 4 **while** $V' \neq \emptyset$ **do**
 - 5 Randomly choose C_r from the k possible clusters of O_d
 - 6 Move a $vd \in V'$ to cluster C_r , if $O_d(vd) \neq r$
 - 7 $V' := V' \setminus \{vd\}$
 - 8 Update QW and vectors of cluster C_r
 - 9 **end**
-

Figure 6 presents an example of the mutation procedure on an individual O_d generated to decode a solution for the Karate network. The mutated individual O_d is a result of the modification of the labels of 6 randomly selected vertices.

O_d

1	2	2	2	2	2	2	2	2	2	2	2	2	1	1	2	2	1	2	1	2	1	1	1	1	1	1	2	2	1	1	1
---	---	---	---	---	---	---	---	---	---	---	---	---	---	---	---	---	---	---	---	---	---	---	---	---	---	---	---	---	---	---	---

$QW(O_d) = 0.1408$

Mutated O_d

2	1	2	2	2	2	2	2	1	2	2	2	1	2	1	1	2	2	1	2	1	2	2	2	2	2	2	1	1	1	2	1	1	2	1	1	1
---	---	---	---	---	---	---	---	---	---	---	---	---	---	---	---	---	---	---	---	---	---	---	---	---	---	---	---	---	---	---	---	---	---	---	---	---

$QW(O_d) = 0.0799$

Figure 6: Example of the mutation procedure on an individual that decodes a solution for the Karate network when $\gamma_1 = \gamma_2 = 0.5$.

Algorithm 6 presents the introduced ensemble algorithm, called *SpecG-EC*. The algorithm has as input G ; \mathcal{NG} ; \mathcal{NP} ; \mathcal{NO} ; p ; IT ; a set of partitions, \mathcal{F} , and a required threshold, τ . A partition from \mathcal{F} is identified by $\mathcal{F}_i, i = \{1, \dots, N\mathcal{F}\}$, and represents the solution achieved by *MOSpecG* for $\gamma_1 = (i - 1) \frac{1}{N\mathcal{F} - 1}, \gamma_2 = 1 - \gamma_1$.

Algorithm 6: *SpecG-EC*

Input : $G, \mathcal{NG}, \mathcal{NP}, \mathcal{NO}, p, IT, \mathcal{F}$ and τ
Output: Ensemble partition EC

- 1 $\mathcal{F}' := \mathcal{F} \setminus \{\mathcal{F}_1, \mathcal{F}_{N\mathcal{F}}\}$
- 2 $e_{ij} :=$ number of times that $\mathcal{F}'_a(i) = \mathcal{F}'_b(j), \forall \mathcal{F}'_a, \mathcal{F}'_b \in \mathcal{F}', \forall i, j \in V$
- 3 $\mathcal{E} := \frac{\mathcal{E}}{|\mathcal{F}'|}$
- 4 $e_{ij} = 0$, if $e_{ij} < \tau, \forall i, j \in V$
- 5 $A := A + \mathcal{E}$
- 6 $\Lambda\mathcal{E}, U\mathcal{E} :=$ Eigen-decomposition of B regarding the p largest eigenvalues in absolute value
- 7 $\chi := \max_{\Lambda\mathcal{E}_{ii}, \forall i} (\Lambda\mathcal{E}_{ii})$
- 8 $k' :=$ number of eigenvalues of B with values larger than or equal to $\sqrt{\chi}$
- 9 $k := \lfloor 1.25k' \rfloor$
- 10 Define vertex vectors rp^i and $rn^i, i \in V$
- 11 $EC :=$ *Memetic Algorithm*($\mathcal{NG}, \mathcal{NP}, \mathcal{NO}, IT, k, rp^i, rn^i, \forall i \in V$)

Line 1 of Algorithm 6 assigns to \mathcal{F}' every solution from \mathcal{F} except those by *MOSpecG* for the pair of values $\gamma_1 = 0, \gamma_2 = 1$ and $\gamma_1 = 1, \gamma_2 = 0$, i.e., \mathcal{F}_1 and $\mathcal{F}_{N\mathcal{F}}$. Let $\mathcal{E} = [e_{ij}] \in \mathbb{R}^{n \times n}$ be a consensus matrix. In lines 2 to 4, \mathcal{E} is defined according to [15]: in line 2, e_{ij} receives the number of times that vertices i and j appear in the same cluster in the partitions from \mathcal{F}' ; in line 3, matrix \mathcal{E} is normalized; and, in line 4, elements from \mathcal{E} below a threshold τ are set to 0 to avoid noisy data.

In order to favor the grouping of vertices that are in the same cluster in the majority of the partitions from \mathcal{F}' , in line 5, the ensemble algorithm adjusts the original graph by adding the consensus matrix to the adjacency matrix.

The ensemble algorithm calculates the eigenvalues and eigenvectors of the original modularity matrix B , in line 6, and estimates the number of clusters, k , in lines 7 to 9, according to Section 3.2. In line 10, the vertex vectors rp^i and $rn^i, i \in V$, are created from the eigenvalues and eigenvectors of B . Finally, *SpecG-EC* calls Algorithm 2 to find the partition EC that maximizes the modularity of the adjusted graph in line 11. The ensemble algorithm returns EC .

5 Computational Experiments

This section discusses the computational experiments performed with *MOSpecG* in real and artificial networks. The expected partitions of these networks are known and, therefore, to evaluate the correlation between the solutions found by the algorithms and the ground truth partitions, we used the measure Normalized Mutual Information (NMI) [4]. The NMI values lie in the range $[0, 1]$ and the higher they are, the more correlated is the pair of partitions. For a comparative analysis, we contrasted the results achieved by *SpecG-EC* and *MOSpecG* for maximizing modularity, i.e., with $\gamma_1 = \gamma_2 = 0.5$, referred to as *MOSpecG-mod*, with those found by the reference graph clustering algorithms: Moga-Net, OSLOM and Infomap.

The algorithm was implemented in C++ using the ARPACK++ library [18] and the experiments were run on a computer with an Intel Core i7-4790S processor with 3.20GHz and 8GB of main memory. The values of the parameters were defined after preliminary tests: $N\mathcal{F} = 11$, $N\mathcal{G} = 50$, $N\mathcal{P} = 5$, $p = \lfloor \frac{n}{10} \rfloor$ and $IT = 1$. Exceptionally for the experiments with real networks, we set $IT = 5$.

We say that a partition F_a dominates a partition F_b if and only if $Q^{IN}(F_a) > Q^{IN}(F_b)$ and $Q^{NULL}(F_a) \leq Q^{NULL}(F_b)$ or if and only if $Q^{IN}(F_a) \geq Q^{IN}(F_b)$ and $Q^{NULL}(F_a) < Q^{NULL}(F_b)$. In the experiments, we present the results including the dominated partitions obtained by *MOSpecG* because some of them had good NMI values. Therefore, we refer to the sets of solutions found by *MOSpecG* as *solution sets* rather than Pareto frontier approximations.

5.1 Real networks

This section shows the results of the experiments with the real benchmark networks: Karate [29], Dolphins [19], Polbooks [13] and Football [10].

Table 1 reports the average results of ten independent executions of *SpecG-EC*, *MOSpecG-mod*, Moga-Net, OSLOM and Infomap to detect communities in real networks. The results presented are the NMI values, the CPU-times in seconds and number of clusters. The standard deviation of the presented values is shown between parentheses. Table 1 also presents the number of clusters in the expected partitions.

As can be seen in Table 1, on the one hand, *SpecG-EC* outperformed Moga-Net in all the networks. On the other hand, *MOSpecG-mod* only found lower NMI values than Moga-Net for the Polbooks network. Moga-Net and Infomap were the only algorithms which did not obtain the expected partition for the Karate network. *SpecG-EC* achieved higher NMI values than all the reference algorithms, including *MOSpecG-mod*, for the Dolphins and Polbooks networks. Furthermore, the number of clusters in the partitions obtained by *SpecG-EC* and *MOSpecG-mod* varied at a maximum of 25% and 43.333%, respectively and

		Network			
		Karate	Dolphins	Polbooks	Football
Number of vertices		34	62	105	115
Number of edges		78	159	441	613
<i>SpecG-EC</i>	NMI	1 (0)	0.889 (0)	0.565 (0.006)	0.864 (0.03)
	CPU-time (s)	0.172 (0.05)	0.33 (0.053)	0.884 (0.131)	1.377 (0.203)
	#Clusters	2 (0)	2 (0)	2.3 (0.483)	9 (1.054)
<i>MOSpecG-mod</i>	NMI	1 (0)	0.662 (0)	0.485 (0.026)	0.876 (0.023)
	CPU-time (s)	0.015 (0.003)	0.025 (0.004)	0.081 (0.015)	0.129 (0.028)
	#Clusters	2 (0)	3 (0)	4.3 (0.483)	9.4 (0.699)
Moga-Net	NMI	0.682 (0.047)	0.538 (0.067)	0.511 (0.054)	0.736 (0.048)
	CPU-time (s)	7.85 (0.627)	11.827 (1.255)	25.231 (2.656)	28.61 (2.888)
	#Clusters	3.9 (0.316)	6.1 (1.449)	5.5 (1.65)	7.8 (1.033)
OSLOM	NMI	1 (0)	0.786 (0.11)	0.558 (0.017)	0.916 (0)
	CPU-time (s)	0.3 (0.483)	0.9 (0.568)	1.2 (0.422)	0.7 (0.483)
	#Clusters	2 (0)	2 (0)	3.7 (0.675)	11 (0)
Infomap	NMI	0.699 (0)	0.519 (0)	0.537 (0)	0.924 (0)
	CPU-time (s)	0.2 (0.422)	0.5 (0.527)	0.4 (0.516)	0.4 (0.516)
	#Clusters	3 (0)	6 (0)	5 (0)	12 (0)
Expected	#Clusters	2	2	3	12

Table 1: NMI, CPU-times and number of clusters achieved by the algorithms for real graphs.

on average, when compared to the expected number of clusters. Thereby, there is empirical evidence suggesting the effectiveness of the proposed algorithm in estimating the number of clusters.

Figure 8 exhibits the *solution sets* achieved by a single execution of *MOSpecG* for the real benchmark networks. This figure illustrates the trade-offs between the two conflicting objectives. Each point is labeled with the NMI value achieved by the corresponding partitions¹.

MOSpecG was able to correctly identify the expected partitions of the Karate network for $\gamma_1 \in \{0.3, 0.4, \dots, 0.8\}$ and $\gamma_2 \in \{0.2, 0.3, \dots, 0.7\}$. On the one hand, *MOSpecG* achieved the highest NMI values for the Dolphins network when $\gamma_1 Q^{IN} > \gamma_2 Q^{NULL}$ and $\gamma_1 > \gamma_2$. On the other hand, it achieved the highest NMI values for the Football and Polbooks networks when $\gamma_2 Q^{NULL} > \gamma_1 Q^{IN}$ and $\gamma_2 > \gamma_1$.

Figures 8(a) and 8(b) show that *SpecG-EC* found partitions whose average NMI values were equal to the partitions from the *solution sets* with the best NMI values for the Karate and Dolphins networks. Regarding the Football network, however, *SpecG-EC* found partitions whose average NMI value was 5.677% worse than the highest NMI value of partitions

¹The NMI values differ from those reported in Table 1 due to the selection of a single execution of the algorithm.

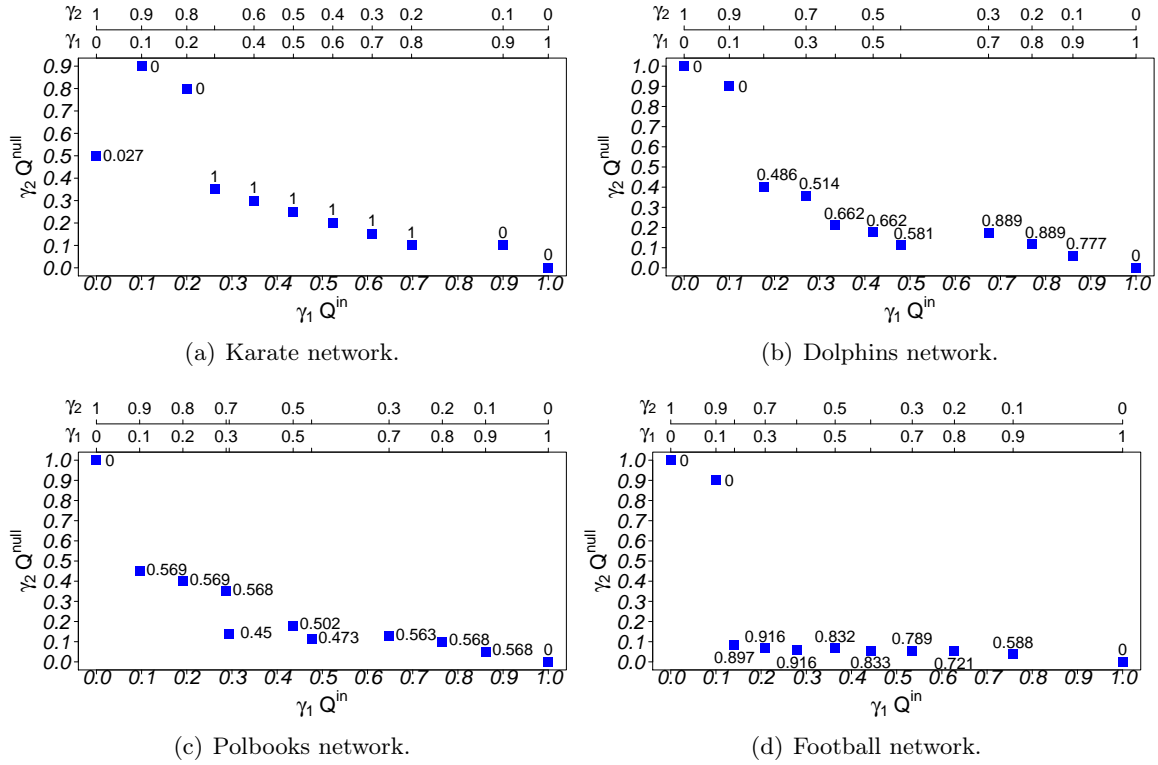


Figure 8: *Solution sets.*

from the *solution set* presented in Figure 8(d). Moreover, the average NMI value of partitions obtained by *SpecG-EC* for the Polbooks network is only 0.703% lower than the highest NMI value of partitions from the *solution set* presented in Figure 8(c).

Figures 9, 10, 11 and 12 illustrate the partitions found by *SpecG-EC* and *MOSpecG-mod* for the Karate, Dolphins, Polbooks and Football networks, respectively. These figures also report the partitions found by *MOSpecG* with the γ_1 and γ_2 values that resulted in the highest NMI values, here referred to as best partitions. Each vertex is identified by its cluster label in these figures.

Figure 9 exhibits the expected partition of the Karate network, found by the proposed algorithm. Figure 10 shows that the ensemble and the best partition obtained by *MOSpecG* for the Dolphins network have the expected number of clusters. The cluster with label 3 from the partition returned by *MOSpecG-mod*, in Figure 10(b), is merged with the cluster with label 1 in the ensemble partition in Figure 10(a). Figure 11 shows that most of the vertices from clusters with labels 3 and 4 in the partition found by *MOSpecG-mod* are merged in, respectively, clusters with labels 1 and 2 in the ensemble partition obtained by *SpecG-EC*. None of the partitions found for the Football network in Figure 12 correctly defined the number of clusters. The differences between the NMI values reported in Figures 11 and 12

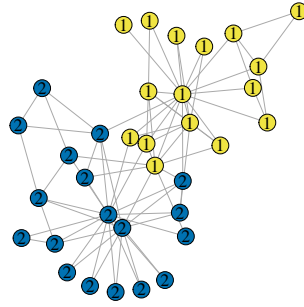
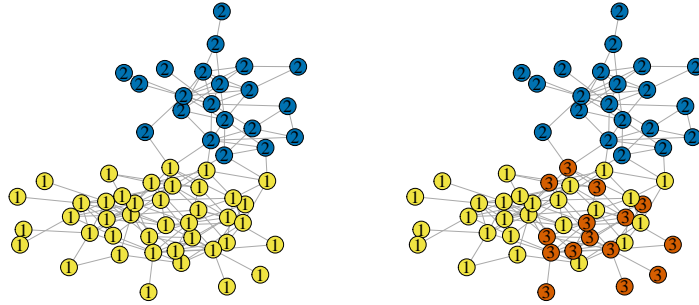


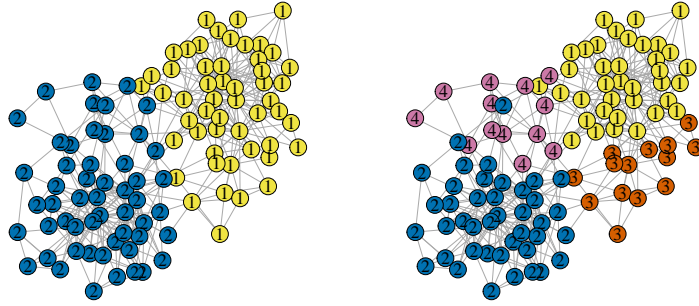
Figure 9: The partition found by *SpecG-EC*, *MOSpecG-mod* and *MOSpecG* with $\gamma_1 \in \{0.3, 0.4, \dots, 0.8\}$ and $\gamma_2 \in \{0.2, 0.3, \dots, 0.7\}$ for the Karate network: NMI value of 1.



(a) The partition found by *SpecG-EC* and the best partition found by *MOSpecG* with $\gamma_1 \in \{0.7, 0.8\}, \gamma_2 \in \{0.2, 0.3\}$: NMI value of 0.889.
 (b) The partition found by *MOSpecG-mod*: NMI value of 0.662.

Figure 10: Dolphins network.

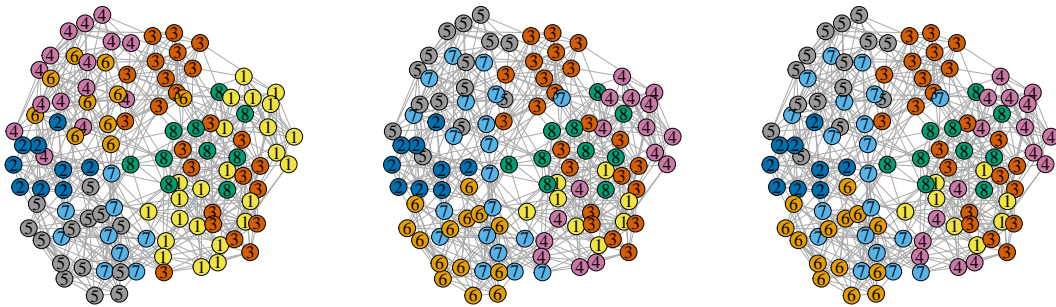
and those presented in Table 1 result from the fact that the figures only report the results of a single execution, whereas the table presents the averages of ten executions.



(a) The partition found by *SpecG-EC* and the best partition found by *MOSpecG* with $\gamma_1 \in \{0.1, 0.2\}, \gamma_2 \in \{0.8, 0.9\}$: NMI value of 0.569.

(b) The partition found by *MOSpecG-mod*: NMI value of 0.502.

Figure 11: Polbooks network.



(a) The partition found by *SpecG-EC*: NMI value of 0.839.

(b) The partition found by *MOSpecG-mod*: NMI value of 0.832.

(c) The best partition found by *MOSpecG* with $\gamma_1 = 0.4, \gamma_2 = 0.6$: NMI value of 0.916.

Figure 12: Football network.

5.2 LFR networks

This experiment used 80 undirected LFR networks [17] with the following characteristics: 1000 vertices; average degree within the range [20, 50]; small-sized communities, whose number of vertices are in the interval [10, 50]; large-sized communities, whose number of vertices are in the interval [20, 100]; and degree of mixture (mixture coefficient) between groups (μ) with values from the set $\{0.1, 0.2, \dots, 0.8\}$.

Figures 13 to 17 display the average results of the algorithms applied to the LFR networks (y-axis) by μ (x-axis). Figures 13(a) and 13(b) present the average NMI values of partitions obtained by *MOSpecG* for, respectively, the small and large-sized community

networks considering each combination of weights γ_1 and γ_2 .

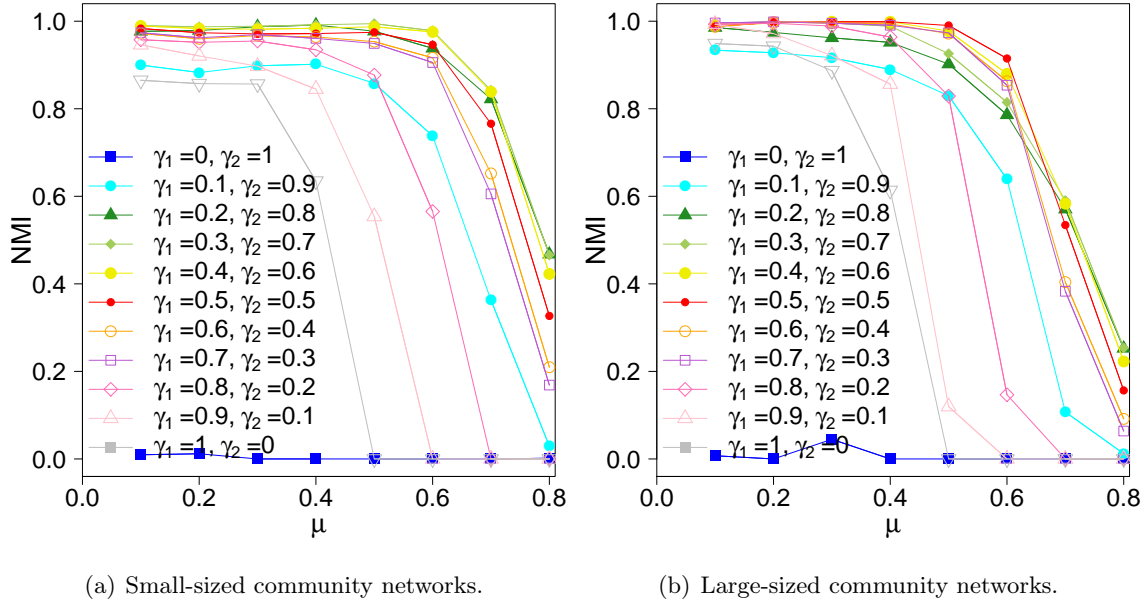


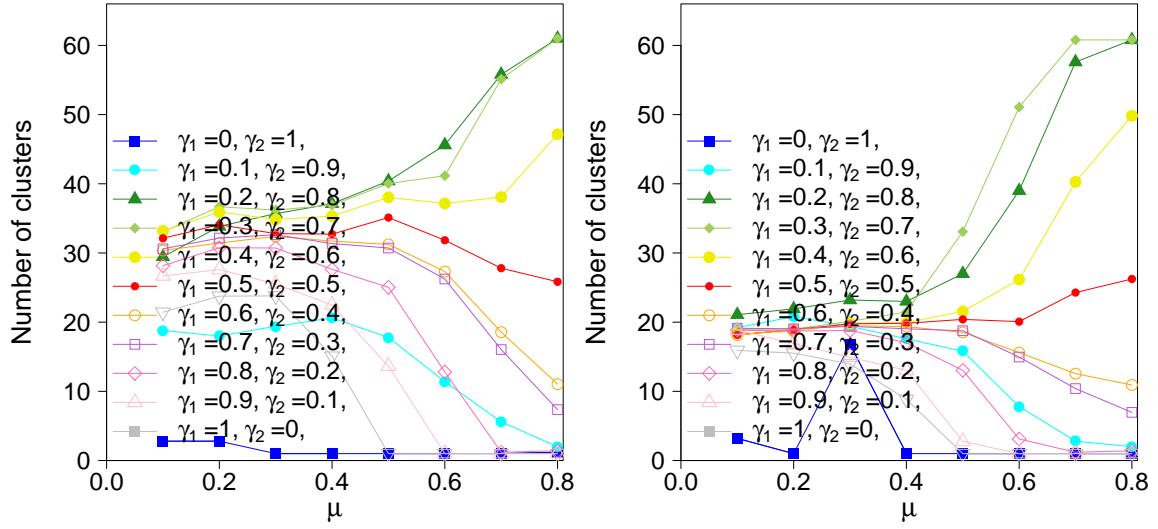
Figure 13: Average NMI values of the partitions obtained by *MOSpecG* considering different values of γ_1 and γ_2 .

As can be noted in Figures 13(a) and 13(b), the values of $\gamma_1 \in \{0.2, 0.3\}$ and $\gamma_2 \in \{0.7, 0.8\}$ resulted in partitions with the highest average NMI values for the networks with $\mu \geq 0.7$. The proposed heuristic presented competitive results when detecting communities in all networks by optimizing the modularity, i.e., when $\gamma_1 = \gamma_2 = 0.5$. The partitions found when considering $\gamma_1 = 0$ and $\gamma_2 = 1$ failed to identify good quality clusters.

Figures 14(a) and 14(b) show the average number of clusters in the partitions from the *solution sets* for, respectively, the small and large-sized community networks. Except for the results when $\gamma_1 = 0, \gamma_2 = 1$, which misidentified the number of clusters, and when $\gamma_1 = 0.1, \gamma_2 = 0.9$, the lower the γ_1 and the larger the γ_2 , the larger the number of clusters. Thereby, the number of communities grows with $\gamma = \frac{\gamma_2}{\gamma_1}$.

Figure 15 presents the average NMI values of the partitions found by *SpecG-EC*, *MOSpecG-mod*, OSLOM, Infomap and Moga-Net whereas Figure 16 shows the respective average CPU-times for the small and large-sized community networks.

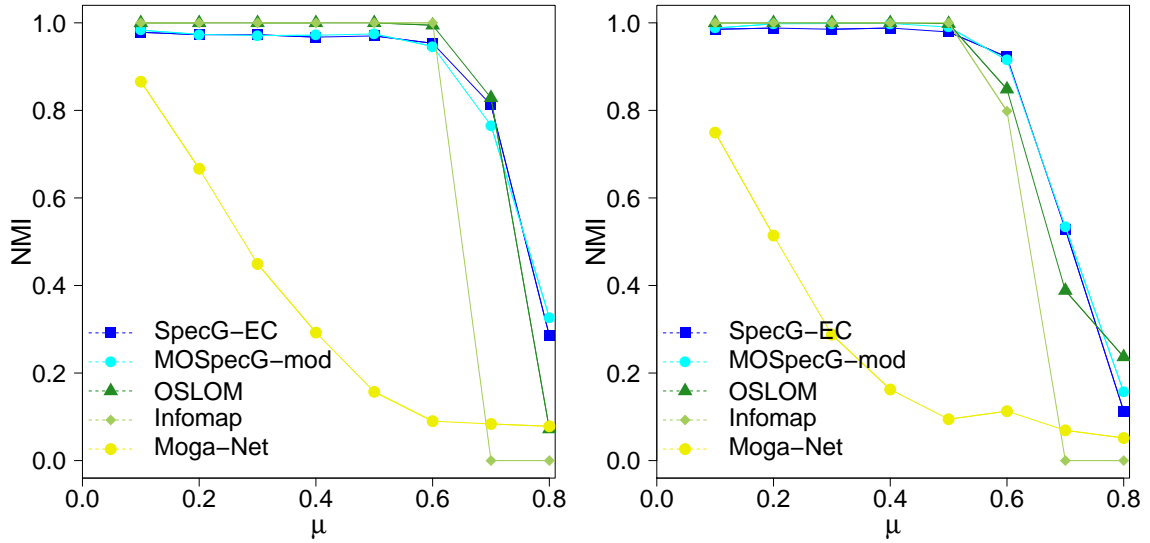
Figure 15 shows that the partitions found by *SpecG-EC* and *MOSpecG-mod* had average NMI values higher than those with the largest modularity found by Moga-Net. Moreover, *SpecG-EC* outperformed *MOSpecG-mod*, Infomap and OSLOM in the small-sized community networks with, respectively, $\mu \in \{0.6, 0.7\}$, $\mu \geq 0.7$ and $\mu = 0.8$. In the small-sized community networks with $\mu \leq 0.6$, *SpecG-EC* obtained partitions whose NMI values were



(a) Small-sized community networks.

(b) Large-sized community networks.

Figure 14: Average number of clusters in the partitions found by *MOSpecG* considering different values of γ_1 and γ_2 .

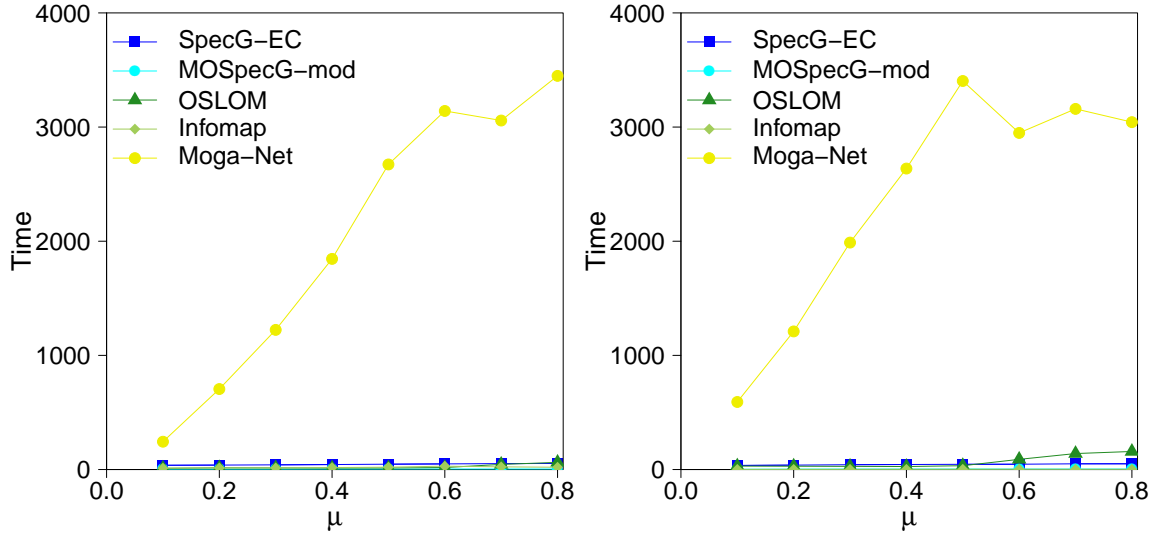


(a) Small-sized community networks.

(b) Large-sized community networks.

Figure 15: Average NMI values achieved by the algorithms.

higher or equal to 0.953. *SpecG-EC* outperformed *MOSpecG-mod*, Infomap and OSLOM in large-sized community networks with, respectively, $\mu = 0.6$, $\mu \geq 0.6$ and $\mu \in \{0.6, 0.7\}$, and achieved NMI values of at least 0.979 in the networks when $\mu \leq 0.5$.



(a) Small-sized community networks.

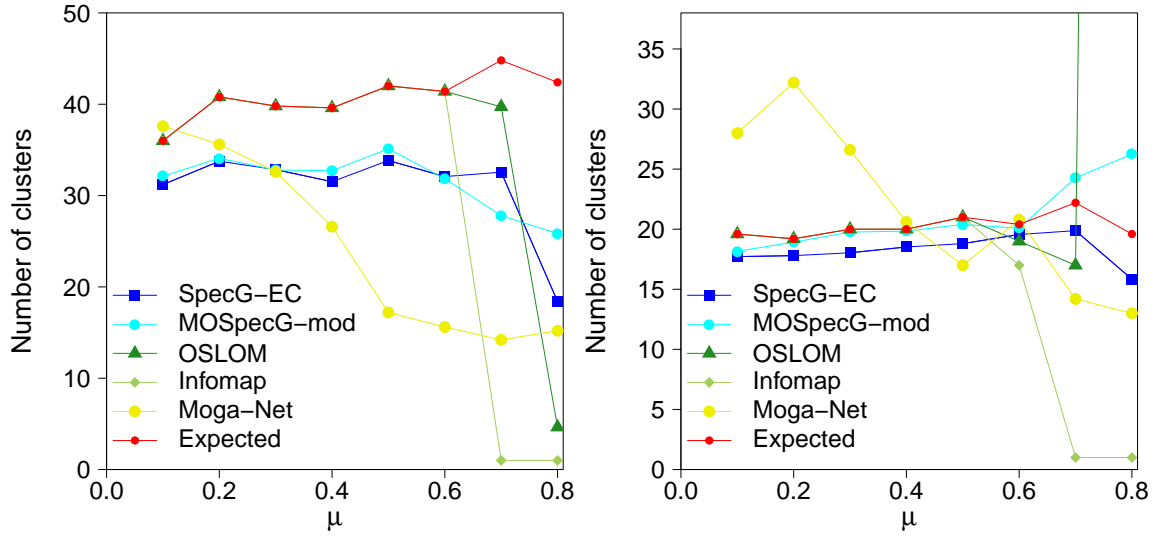
(b) Large-sized community networks.

Figure 16: Average CPU-times (s) required by the algorithms.

MOSpecG-mod and Infomap were the algorithms with the lowest CPU-times in networks with, respectively, small and large-sized community networks. Nonetheless, *SpecG-EC* was from 6 to 64 times faster than Moga-Net in all the networks. On the one hand, *SpecG-EC* was faster than OSLOM in the large-sized community networks with $\mu \geq 0.6$. On the other, it required from 1.18 to 3.056 times more than the CPU time required by OSLOM in the remaining networks. Because *MOSpecG-mod* was approximately 13.286 times faster than *SpecG-EC*, it was also faster than OSLOM in all the networks.

Figure 17 shows the number of clusters obtained by the algorithms in the partitions and in the expected partitions.

As can be seen in Figure 17, Moga-Net obtained the partitions with the worst estimation of numbers of clusters with regard to the expected partitions. On the one hand, OSLOM and Infomap found partitions whose number of clusters is exactly the expected in small and large-sized community networks with, respectively, $\mu \leq 0.6$ and $\mu \leq 0.5$. On the other hand, as opposed to *SpecG-EC* and *MOSpecG-mod*, Infomap failed to identify the number of clusters in the networks with $\mu \geq 0.7$; and OSLOM obtained partitions with worse estimations of number of clusters with regard to the expected partitions than both versions of the proposed algorithm for small and large-sized community networks with, respectively, $\mu = 0.8$ and $\mu \geq 0.7$. In particular, despite presenting slightly better NMI values than *SpecG-EC* and *MOSpecG-mod* for large-sized community network with $\mu = 0.8$, OSLOM wrongly identified approximately 381 clusters, on average, more than the expected.



(a) Small-sized community networks.

(b) Large-sized community networks.

Figure 17: Average number of clusters found by the algorithms in the partitions and in the expected partitions.

6 Final Remarks and Future Works

This paper presented a novel spectral decomposition of modularity to clustering graphs through a multi-objective memetic algorithm called *MOSpecG*. In addition, it introduced an ensemble algorithm, here called *SpecG-EC*, that combines partitions obtained by *MOSpecG* to provide a single partition.

The results of computational experiments using real and LFR networks showed that *SpecG-EC* and the version of *MOSpecG* that maximizes modularity, named *MOSpecG-mod*, outperformed a multi-objective genetic algorithm found in the literature and presented reasonable running times when compared to reference algorithms. The *SpecG-EC* and *MOSpecG-mod* found partitions more similar to the expected ones than state-of-the-art mono-objective algorithms in artificial networks with higher mixture coefficients and satisfactory results in the remaining artificial networks. In particular, *SpecG-EC* performed better in artificial large-sized community networks and outperformed state-of-the-art mono-objective algorithms in two real networks.

Because *SpecG-EC* obtained better results than *MOSpecG-mod* for most of the networks, we can conclude that the ensemble strategy outperformed the maximization of the classical modularity. Nonetheless, *SpecG-EC* constructs its solution using partitions found by *MOSpecG* and thus is slower than *MOSpecG-mod*. The experiments also suggested that both the ensemble and the modularity maximization version of the proposed algorithm pro-

vide a reasonable number of clusters in real and artificial networks.

The empirical finding that some partitions found by *MOSpecG-mod* were more similar to the expected partitions than both the modularity maximization and ensemble partitions suggests advantages of studying the duality between the terms of the modularity using multi-objective graph clustering algorithms. In this sense, as future work, we intend to further improve the results achieved by *SpecG-EC* by studying more effective procedures to select partitions from multi-objective problems for the ensemble. Another research direction would be to reduce the computational cost of the spectral decomposition to make SpecG-EC more effective in detecting communities in larger graphs. Because large graphs are known to be sparse, a first attempt to reduce such computational time would involve employing the spectral decomposition of the flow matrix as the fitness function.

Acknowledgments

The authors would like to acknowledge the foundings provided by São Paulo Research Foundation (FAPESP), grant numbers: 2016/22688-2 and 2015/21660-4; and by Conselho Nacional de Desenvolvimento Científico e Tecnológico (CNPq), grant numbers: 448614/2014-6 and 308708/2015-6. The second author also thanks Leonardo V. Rosset for giving her a hand.

References

- [1] J. W. Berry, B. Hendrickson, R. A. LaViolette, and C. A. Phillips. Tolerating the community detection resolution limit with edge weighting. *Physical Review E*, 83(5): 056119, 2011.
- [2] U. Brandes, D. Delling, M. Gaertler, R. Gorke, M. Hofer, Z. Nikolosk, and D. Wagner. On modularity clustering. *IEEE Transactions on Knowledge and Data Engineering*, 20: 172–188, 2008.
- [3] D. M. Carvalho, H. Resende, and M. C. Nascimento. Modularity maximization adjusted by neural networks. In *International Conference on Neural Information Processing*, pages 287–294. Springer, 2014.
- [4] L. Danon, A. Diaz-Guilera, J. Duch, and A. Arenas. Comparing community structure identification. *Journal of Statistical Mechanics: Theory and Experiment*, 2005(09): P09008, 2005.
- [5] R. K. Darst, Z. Nussinov, and S. Fortunato. Improving the performance of algorithms to find communities in networks. *Physical Review E*, 89(3):032809, 2014.

- [6] P. De Meo, E. Ferrara, G. Fiumara, and A. Provetti. Enhancing community detection using a network weighting strategy. *Information Sciences*, 222:648–668, 2013.
- [7] K. Deb, A. Pratap, S. Agarwal, and T. Meyarivan. A fast and elitist multiobjective genetic algorithm: NSGA-II. *IEEE Transactions on Evolutionary Computation*, 6(2): 182–197, 2002.
- [8] M. Ehrgott. *Multicriteria optimization*, volume 491. Springer Science & Business Media, 2005.
- [9] S. Fortunato and M. Barthélemy. Resolution limit in community detection. *Proceedings of the National Academy of Sciences*, 104(1):36, 2007.
- [10] M. Girvan and M. E. Newman. Community structure in social and biological networks. *Proceedings of the National Academy of Sciences*, 99(12):7821–7826, 2002.
- [11] M. Gong, L. Ma, Q. Zhang, and L. Jiao. Community detection in networks by using multiobjective evolutionary algorithm with decomposition. *Physica A: Statistical Mechanics and its Applications*, 391(15):4050–4060, 2012.
- [12] A. Khadivi, A. A. Rad, and M. Hasler. Network community-detection enhancement by proper weighting. *Physical Review E*, 83(4):046104, 2011.
- [13] V. Krebs. A network of books about recent us politics sold by the online bookseller amazon. com, 2008. URL <http://www.orgnet.com>.
- [14] F. Krzakala, C. Moore, E. Mossel, J. Neeman, A. Sly, L. Zdeborová, and P. Zhang. Spectral redemption in clustering sparse networks. *Proceedings of the National Academy of Sciences*, 110(52):20935–20940, 2013.
- [15] A. Lancichinetti and S. Fortunato. Consensus clustering in complex networks. *Scientific Reports*, 2:336, 2012.
- [16] A. Lancichinetti, S. Fortunato, and F. Radicchi. Benchmark graphs for testing community detection algorithms. *Physical Review E*, 78(4):046110, 2008.
- [17] A. Lancichinetti, F. Radicchi, J. J. Ramasco, and S. Fortunato. Finding statistically significant communities in networks. *PLOS ONE*, 6, 04 2011.
- [18] R. B. Lehoucq, D. C. Sorensen, and C. Yang. *ARPACK users' guide: solution of large-scale eigenvalue problems with implicitly restarted Arnoldi methods*, volume 6. Siam, 1998.

- [19] D. Lusseau, K. Schneider, O. Boisseau, P. Haase, E. Slooten, and S. Dawson. The bottlenose dolphin community of doubtful sound features a large proportion of long-lasting associations. *Behavioral Ecology and Sociobiology*, 54(4):396–405, 2003.
- [20] M. C. V. Nascimento, F. M. B. De Toledo, and A. C. P. L. F. Carvalho. Consensus clustering using spectral theory. In *International Conference on Neural Information Processing*, pages 461–468. Springer, 2008.
- [21] M. E. Newman. Finding community structure in networks using the eigenvectors of matrices. *Physical Review E*, 74(3):036104, 2006.
- [22] M. E. Newman and M. Girvan. Finding and evaluating community structure in networks. *Physical Review E*, 69(2):026113, 2004.
- [23] C. Pizzuti. A multiobjective genetic algorithm to find communities in complex networks. *IEEE Transactions on Evolutionary Computation*, 16(3):418–430, 2012.
- [24] J. Reichardt and S. Bornholdt. Statistical mechanics of community detection. *Physical Review E*, 74(1):016110, 2006.
- [25] M. Rosvall and C. T. Bergstrom. An information-theoretic framework for resolving community structure in complex networks. *Proceedings of the National Academy of Sciences*, 104(18):7327–7331, 2007.
- [26] C. P. Santos, D. M. Carvalho, and M. C. Nascimento. A consensus graph clustering algorithm for directed networks. *Expert Systems with Applications*, 54:121–135, 2016.
- [27] C. Shi, Z. Yan, Y. Cai, and B. Wu. Multi-objective community detection in complex networks. *Applied Soft Computing*, 12(2):850–859, 2012.
- [28] D. J. Watts and S. H. Strogatz. Collective dynamics of ‘small-world’ networks. *Nature*, 393(6684):440–442, 1998.
- [29] W. W. Zachary. An information flow model for conflict and fission in small groups. *Journal of Anthropological Research*, 33(4):452–473, 1977.
- [30] K. R. Žalik and B. Žalik. Multi-objective evolutionary algorithm using problem-specific genetic operators for community detection in networks. *Neural Computing and Applications*, pages 1–14, 2017.
- [31] X. Zhang and M. Newman. Multiway spectral community detection in networks. *Physical Review E*, 92(5):052808, 2015.